# FULL PAPER

# Diffusion-weighted imaging: determination of the best pair of *b*-values to discriminate breast lesions

[1,2]L NOGUEIRA, MSc, [3]S BRANDÃO, MSc, [4]E MATOS, MSc, [5]R G NUNES, PhD, [3]J LOUREIRO, MD, [5]H A FERREIRA, MD, PhD and [2]I RAMOS, MD, PhD

[1]Department of Radiology, School of Allied Health Sciences, Oporto Polytechnic Institute (ESTSP/IPP), Vila Nova de Gaia, Portugal
[2]Department of Radiology, Hospital de São João/Faculty of Medicine of Porto University (FMUP), Porto, Portugal
[3]MRI Unit, Department of Radiology, Hospital de São João, Porto, Portugal
[4]Department of Health Community, Institute of Biomedical Sciences Abel Salazar of Porto University (ICBAS), Porto, Portugal
[5]Institute of Biophysics and Biomedical Engineering (IBEB), Faculty of Sciences, University of Lisbon, Campo Grande, Lisboa, Portugal

Address correspondence to: Dr Maria Luísa Nogueira
E-mail: *mlpnogueira@med.up.pt*

**Objective:** In breast diffusion-weighted imaging (DWI), the apparent diffusion coefficient (ADC) is used to discriminate between malignant and benign lesions. As ADC estimates can be affected by the weighting factors, our goal was to determine the optimal pair of *b*-values for discriminating breast lesions at 3.0 T.

**Methods:** 152 females with 157 lesions (89 malignant and 68 benign) underwent breast MRI, including a DWI sequence sampling six *b*-values 50, 200, 400, 600, 800 and 1000 s mm$^{-2}$. ADC values were computed from different pairs of *b*-values and compared with ADC obtained by fitting the six *b*-values using a mono-exponential diffusion model (ADC$_{all}$). Cut-off ADC values were determined and diagnostic performance evaluated by receiver operating characteristic analysis using Youden statistics. Mean ADCs were determined for normal tissue and lesions. Differences were evaluated by lesion and histological types.

**Results:** Considering the cut-off values 1.46 and 1.49 × 10$^3$ mm$^2$ s$^{-1}$, the pairs 50, 1000 and 200, 800 s mm$^{-2}$ showed the highest accuracy, 77.5% and 75.4% with areas under the curve 84.4% and 84.2%, respectively. The best pair for ADC quantification was 50, 1000 s mm$^{-2}$ with 38/49 true-negative and 69/89 true-positive cases respectively; mean ADCs were 1.86 ± 0.46, 1.77 ± 0.37 and 1.15 ± 0.46 × 10$^{-3}$ mm$^2$ s$^{-1}$ for normal, benign and malignant lesions. There were no significant differences in these ADC values when compared with ADC$_{all}$ (ADC calculated from the full set of *b*-values) [difference = 0.0075 × 10$^{-3}$ mm$^2$ s$^{-1}$; confidence interval 95%: (−0.0036; 0.0186); *p* = 0.18].

**Conclusion:** The diagnostic performance in differentiating malignant and benign lesions was most accurate for the *b*-value pair 50, 1000 s mm$^{-2}$.

**Advances in knowledge:** The best *b*-value pair for lesion discrimination and characterization through ADC quantification was 50, 1000 s mm$^{-2}$.

Over the past years, MRI has been used to study breast lesions,[1–3] with clinical recommendations established for its application.[4–6] Interpretation of conventional breast MRI is based on morphological and kinetic descriptors.[7] However, sometimes lesions present features that limit accurate characterization and diagnostic performance. The use of diffusion-weighted imaging (DWI) has helped to overcome this limitation, with improved specificity and accuracy for lesion detection and discrimination,[8,9] especially when combined with dynamic MRI.[10,11] To evaluate water mobility in normal breast tissue and lesions, the apparent diffusion coefficient (ADC) can be quantified from the signal intensity (SI) loss between two or more *b*-values.[12,13] ADC calculation is based on the logarithmic transformation of the SI loss over time, expressed by ADC = −1/(b2 − b1) log (Sb2/Sb1), where Sb1 and Sb2 represent the SI measured for *b*-values b1 and b2, respectively.[14]

ADC estimates are expected to become more accurate as the number of *b*-values increases.[14] However, a study by Bogner et al[15] showed only minor improvement in ADC precision when the number of *b*-values was increased from two up to ten. Given that the acquisition time is proportional to the number of *b*-values, a compromise must be sought to minimize it while maintaining adequate ADC precision. Another issue to consider is that the echo-time (TE) increases with the highest *b*-value used, resulting in a lower signal-to-noise ratio (SNR) owing to transverse relaxation.

The typical highly cellular composition of malignant lesions impedes water mobility,[16] and so they should exhibit a higher SI on DWI and a lower ADC value than benign lesions.[17,18] However, it is important not to neglect the intrinsic $T_2$ weighting of diffusion images. A tissue change that has a longer

or shorter $T_2$ relaxation would also lead to an increased or decreased SI (respectively), which could erroneously be interpreted as being related to changes in diffusion properties. Prolonged $T_2$ values in certain tissues, such as water in cysts, cause a $T_2$ shine through effect on DWI, whereas $T_2$ shortening results in $T_2$ blackout effects.[14,19,20] To avoid these confounds, it is essential to compute quantitative ADC maps and use them to analyse the areas with high SI on high $b$-value images as stated by Koh and Collins[14].

In the case of simple cysts, ADC is increased because restriction to water mobility is scarce owing to low cellularity.[8] In comparison, complex cysts present proteins and blood in their matrix that lead to a low ADC.[13] Finally, benign lesions have higher ADC than malignant ones because of their less compact cellularity.[17,21]

Le Bihan et al[22] attributed SI differences in lesions to changes in the intra- and extracellular compartments' architecture and to modified microcirculation, which can be affected as a result of the neovascularization process allied to solid lesion growth. The SI loss related to microcirculation, which results from intravoxel incoherent motion (IVIM), can be estimated by including low $b$-value images and a bi-exponential model[23,24] to account for this "pseudo-diffusion coefficient". Since this coefficient is typically an order of magnitude higher than the diffusion coefficient, the impact of IVIM should be considered when choosing the minimum $b$-value. For a sufficiently high minimum $b$-value, the perfusion contribution may be ignored and a mono-exponential model used to describe the data. As for the highest $b$-value, it should be chosen so as to provide adequate suppression of water signal from normal fibroglandular tissue and maximum breast lesion visibility.[23]

As far as we are aware, the post-processing software available on clinical scanners employs a mono-exponential model to fit the SI decay.[14] This model does not account for perfusion, which means that the estimated ADC value will be affected by the perfusion fraction to a degree that depends on the choice of the $b$-values.

In addition, a recent meta-analysis[25] highlighted the fact that there is no standard set of $b$-values to discriminate benign from malignant lesions. Some studies combined low 0 or 50 s mm$^{-2}$ and high 1000–1500 s mm$^{-2}$ $b$-values,[15,25] whereas others used a larger set of $b$-values to calculate the ADC.[26,27] The use of $b = 800$ s mm$^{-2}$ and higher seems to increase the sensitivity for lesion differentiation.[27,28] However, ADC thresholds are highly variable in the literature, ranging from 1.10 to $1.61 \times 10^{-3}$ mm$^2$ s$^{-1}$.[25] Several factors may contribute to that, such as lesion heterogeneity between the samples; different field strengths and acquisition protocols across the studies (including $b$-values); and image analysis procedure including region of interest (ROI) size and delineation criteria.[18,26,29]

The purpose of our study was to identify the optimal pair(s) of $b$-values, for which the estimated ADC shows the best accuracy for lesion discrimination at 3.0 T, aiming to minimize acquisition time.

## METHODS AND MATERIALS
### Subjects and lesions
A prospective study was conducted between July 2009 and October 2012. All females with clinical indication for breast MRI who fulfilled the inclusion criteria were asked to participate in this study. Data presented here are included in a wider investigation, and the study has received approval from the Ethics Committee of Hospital São João, Porto, Portugal [protocol: Comissão de Etica para a Saúde (CES) 276/13]. Written informed consent was obtained from all patients.

Within this period, 219 breast MRI examinations (182 consecutive patients) were performed. 30 patients were evaluated more than once. Clinical indications to perform breast MRI included pre-operative evaluation, pre- and post-neoadjuvant chemotherapy, positive surgical margins, post breast conservation, unknown primary malignancy, breast cancer screening, equivocal mammographic and/or ultrasound features, therapeutic monitoring, follow-up after surgery and breast cancer recurrence.

Exclusion criteria were (1) patients undergoing chemotherapy or/and radiotherapy at the time of the examination or having received treatment within a period shorter than 24 months ($n = 8$); (2) having been submitted to surgery within less than 6 months ($n = 10$); (3) having finished hormone replacement therapy within less than 24 months ($n = 5$); (4) having breast implants ($n = 2$); and (5) females whose images evidenced relevant motion artefacts ($n = 5$) during the examination.

Lesions were included in the DWI analysis if (1) the minimum size was $\geq 0.7$ cm in dynamic contrast-enhanced (DCE) MRI; (2) proven histological result was available; and (3) females had previous 2-year follow-up with mammography, ultrasound or MRI.

For the pre-menopausal females, the MR examination was performed between the 7th and the 14th day of the menstrual cycle to minimize the enhancement on the fibroglandular tissue owing to gadolinium injection.[30] For females who had undergone needle biopsy, a minimum interval of 10 days before the MRI examination was imposed to reduce potential SI changes due to haemorrhages and/or oedema. Finally, simple cysts were excluded and ignored, as their high ADC would have lead to a bias in the results, increasing ADC values of the benign lesions group.

### Acquisition protocol
The examinations were performed using a 3.0 T system (MAGNETOM® Trio Tim System; Siemens Healthcare, Erlangen, Germany) equipped with a dedicated four-channel phase-array coil (Invivo Corporation, Orlando, FL). Patients rested in the prone position. Table 1 presents the main parameters of the scanning protocol.

DWI was performed before the DCE pulse sequence with the sensitization gradients applied in the $x$, $y$ and $z$ directions to generate three-scan-trace images. Eight $b$-values were sampled 50, 200, 400, 600, 800, 1000, 2000 and 3000 s mm$^{-2}$. In this study, we limited the analysis to the range of $b$-values for which the assumption that water diffusion follows a Gaussian distribution can be considered to be valid; the $b$-values included in the analysis therefore ranged from 50 to 1000 s mm$^{-2}$ and a mono-exponential fitting of the signal was performed.[31] For the higher $b$-values 2000 and 3000 s mm$^{-2}$, a non-Gaussian model needs to be considered[32] and so ADC quantification using a mono-exponential fitting incorporating these values would not have been appropriate.

Table 1. Scanning MRI protocol

| Parameters | Conventional pre-contrast | | | DWI-SPAIR | Dynamic | Post-contrast |
|---|---|---|---|---|---|---|
| Sequence | $T_2$W TSE | $T_1$W 3D FLASH | $T_2$W TSE | Single-shot EPI | $T_1$W 3D FLASH | $T_1$W 3D FLASH |
| Orientation | Axial bilateral | Sagittal | Sagittal | Sagittal | Axial bilateral | Sagittal |
| Repetition time/echo time (ms) | 4990/88 | 17/4.9 | 4920/67 | 4900/106 | 3.77/1.42 | 7.8/3.9 |
| Inversion time (ms) | – | – | 210 | – | – | – |
| Fat suppression | – | – | STIR | SPAIR | SPAIR | Water excitation |
| Field of view (mm$^2$) | $320 \times 320$ | $200 \times 200$ | $200 \times 200$ | $250 \times 250$ | $320 \times 320$ | $160 \times 160$ |
| Matrix | $512 \times 384$ | $275 \times 384$ | $448 \times 314$ | $84 \times 128$ | $358 \times 448$ | $256 \times 256$ |
| Slice thickness | 4 | 2 | 4 | 5 | 0.9 | 0.9 |
| Number of slices | 26 | 64 | 26 | 16 | 160 | 144 |
| Number of excitations | 2 | 1 | 2 | 3 | 1 | 1 |
| Bandwidth (Hz per pixel) | 305 | 430 | 248 | 1628 | 490 | 450 |
| Scan time (min) | 2:06 | 3:49 | 4:26 | 5:58 | 4:32 | 3:12 |
| *b*-values (s mm$^{-2}$) | – | – | – | 50, 200, 400, 600, 800, 1000, 2000 and 3000 | – | – |

3D, three dimensional, DWI-SPAIR, diffusion-weighted imaging with spectrally adiabatic inversion–recovery; EPI echo-planar imaging; T1 3D FLASH, three dimensional gradient echo fast low angle shot; $T_1$W, $T_1$ weighted; $T_2$ W, $T_2$ weighted; TSE, turbo spin echo; STIR, short tau inversion recovery.

## Image analysis

All the images were processed in the scanner workstation (Syngo® Multimodality, Siemens Healthcare) using the commercial software (Syngo MR V17A, work in progress). Conventional MRI data were interpreted using the Breast Imaging Reporting and Data System MRI.[7] Lesion size was measured on the DCE images considering its highest dimension using the ruler function.

Two researchers retrospectively analysed the diffusion-weighted (DW) images in consensus. At the time of DWI analysis, readers were blinded to histological results. Each lesion was drawn in the DW images based on the MRI report and using $T_2$ weighted, early subtracted DCE and the post-contrast images, serving as a roadmap to place the ROI. The slice showing the lesion's highest dimension and the best definition of its margins was selected. To measure lesion SI for each *b*-value, images at $b = 400\,\text{s mm}^{-2}$ were selected and 0.25 cm$^2$ fixed size ROI drawn in the most hyperintense area of the lesion and then copied to all others. When using this *b*-value, the contrast between the lesion core and its outer limits is still high, facilitating ROI placement. ROIs were drawn avoiding areas of fibroglandular tissue, as well as necrotic and cystic areas. In females with unilateral lesions, the normal glandular tissue ROI was drawn in the contralateral breast. ROIs were also placed using $b = 400\,\text{s mm}^{-2}$ images. Mean value and standard deviation of the SI within the ROI were recorded for each *b*-value.

## Apparent diffusion coefficient quantification

For normal tissue and lesions, the ADC maps were calculated using (a) the six *b*-values 50, 200, 400, 600, 800, 1000 s mm$^{-2}$ and (b) considering different pairs of *b*-values minimum *b*-value was 50, 200 or 400 s mm$^{-2}$.

When using the six *b*-values, the ADC values ($\text{ADC}_{\text{all}}$) were determined by fitting the linearized version of the mono-exponential model to the data,[33] using the program Excel® (Microsoft, Redmond, WA):

$$S(b) = S_0 \exp(-\,\text{ADC}_{\text{all}} \cdot b) \Rightarrow \ln[S(b)] = \ln[S_0] - \text{ADC}_{\text{all}} \cdot b \quad (1)$$

where $S_0$ is the MRI signal without diffusion-weighted sensitization ($b = 0\,\text{s mm}^{-2}$), and $S(b)$ represents the SI measured for each *b*-value.

When only a pair of *b*-values was used, the ADC was estimated for the nine resulting combinations, using Equation (2):

$$\text{ADC} = \frac{\ln[S(b_1)] - \ln[S(b_2)]}{b_2 - b_1} \quad (2)$$

where $b_1$ and $b_2$ were the two *b*-values considered.

Additionally, for each lesion, the relative difference ($\Delta_{\text{rel}}$) in the ADC value was calculated for each pair of *b*-values as:

$$\Delta_{\text{rel}} = \frac{|\text{ADC} - \text{ADC}_{\text{all}}|}{\text{ADC}_{\text{all}}} \quad (3)$$

## Statistical analysis

A descriptive analysis was performed, by patients and lesion types. For each *b*-value combination, mean ADC values were computed

for normal tissue and solid benign and malignant lesions. The Kolmogorov–Smirnov test was used to verify the normality of the data. The Mann–Whitney test was used to assess the differences in ADC values between lesion type (benign and malignant) and between normal tissue and malignant and benign lesions.

The best pairs of $b$-values were identified as the combinations that showed a $\Delta_{rel} < 6\%$. It was also considered imperative that the corresponding ADC values showed no significant statistical difference when compared with $ADC_{all}$. The pair combinations of $b$-values that did not fulfil both criteria were excluded from the analysis. The Wilcoxon test was used to compare $ADC_{all}$ with the ADC values estimated from $b$-value pairs.

The ADC cut-off for the candidate's $b$-value combinations and $ADC_{all}$ were calculated considering Youden statistics and the minimal distance between the receiver operating characteristic (ROC) curves and the ideal point of coordinates (0, 1), where both the sensitivity and specificity have a maximum value of 1.

For the best $b$-value pairs, false-positive and false-negative, true-positive and true-negative rates were calculated. Wilcoxon signed-rank test (paired sample) was used to compare ADC values by histological type for the best pair combinations.

Data were analysed using the PASW® Statistics v. 20 software (Hong Kong), with statistical significance set at $p < 0.05$.

## RESULTS

### Subject and lesion characteristics

152 females with 157 lesions met the inclusion criteria for image analysis. The mean patient age was $49.1 \pm 2.5$ years (range, 21–82 years). 83 patients were pre-menopausal.

From the 157 lesions, 83 were diagnosed by surgical excision and 38 by needle biopsy, while 36 were accepted to be benign and classified based on the morphological/kinetic features and dimensional stability as observed by mammography, ultrasound and/or MRI during a 2-year follow-up. 89 lesions were classified as malignant: 9 ductal carcinoma *in situ* (DCIS), 47 invasive ductal carcinoma (IDC), 4 lobular carcinoma *in situ*, 20 invasive lobular carcinoma (ILC), 1 mucinous carcinoma and 8 other malignant lesions not otherwise specified (NOS).

68 lesions were benign and included: 24 fibroadenomas (FAs), 7 epithelial proliferative lesions (EPLs), 3 papillomas (PAs), 19 cysts (Cs), 2 hamartomas (HAs) and 13 other benign lesions [fibrocystic changes (FCs), complex sclerosing adenosis (CSA) and complex cyst lesion]. 36 of these benign lesions were evaluated by follow-up and included 9 FAs; 1 EPL, 2 HAs, 8 FCs and 16 cysts. All simple cysts were excluded from the final analysis.

The mean size for benign and malignant lesions were $15.4 \pm 11.4$ mm and $22.2 \pm 13.7$ mm, respectively, ranging from 7 to 78 mm.

### ADC values and differences by tissue type

Table 2 illustrates the descriptive analysis for the mean ADC in normal tissue and solid benign and malignant lesions for all the combinations studied and differences in ADCs between tissue types for each combination of $b$-values.

Results showed significant differences in the ADC between benign and malignant lesions ($p < 0.001$). For all the $b$-value combinations, malignant lesions showed lower ADC values when compared with benign ones.

### Determination of the best pair of $b$-values

Table 3 summarizes the statistics for determining the best pair of $b$-values, including $\Delta_{rel}$ averaged among all lesions and comparison between $ADC_{all}$ and ADC values estimated from the $b$-value pairs.

The pairs 50, 800; 50, 1000; 200, 800 and 200, 1000 s mm$^{-2}$ showed the lowest $\Delta_{rel}$ (the sum of their relative frequencies was 79%), corresponding to a $\Delta_{rel} < 6\%$. Although, the pairs 50, 800 and 200, 1000 s mm$^{-2}$ presented a low variability with $\Delta_{rel} < 6\%$, significant differences were found when comparing the ADC values estimated with $ADC_{all}$ and, for this reason, these pairs were excluded from subsequent analysis.

The combination 50, 1000 s mm$^{-2}$ provided the best results, with a mean $\Delta_{rel} < 3\%$ and no significant differences in the ADC when compared with $ADC_{all}$ ($p = 0.152$). The ADC calculated from the pair 200, 800 s mm$^{-2}$ also showed no significant differences relative to $ADC_{all}$ ($p = 0.866$), but displayed higher mean $\Delta_{rel}$ (5.2%).

### Diagnostic accuracy for the optimal pairs of $b$-values

The ADC cut-offs (for solid benign and malignant lesions) using $ADC_{all}$, 50, 1000 and 200, 800 s mm$^{-2}$ were calculated to assess sensitivity and specificity. Figure 1 presents the ROC curves for the best $b$-value combination and $ADC_{all}$.

To compare the performance of each pair for lesion discrimination once an ADC cut-off had been established, their sensitivity, specificity, false and true rates were calculated (Table 4).

Regarding the two tested pairs, 50, 1000 s mm$^{-2}$ showed the highest accuracy (77.5%; AUC = 84.4%), followed by 200, 800 s mm$^{-2}$ (75.4%; AUC = 84.2%).

The pair 50, 1000 s mm$^{-2}$ showed the lowest number of false-negative and false-positive cases. False-negative cases were predominantly IDC with *in situ* component and necrosis areas (7), ILC (8), DCIS (3) and other malignant NOS (2). Inspecting the lesion sizes, for the false-negative cases, these ranged from 18 to 29 mm for IDC, ILC ranging from 12 to 18 mm, DCIS ranged from 9 to 12 mm and NOS with 18 and 25 mm.

False-positive cases were 1 PA, 6 FA, 2 CSA and 2 EPL with fibroblastic/miofibroblastic component. The largest dimension for the PA was 8 mm with FA ranging from 8 to 15 mm. The sizes of the remaining false-positive lesions were of 9 and 10 mm for CSA and 9 and 11 mm for the two EPL.

Figure 2a–c presents the ADC distribution for the lesion type and normal glandular tissue for $ADC_{all}$ and the two best pairs of $b$-values.

Table 2. Apparent diffusion coefficient (ADC) values for normal tissue, solid benign and malignant lesions *vs b*-value combinations and differences for each pair combination between tissue types

| *b*-values (s mm$^{-2}$) | ADC value ($\times 10^{-3}$ mm$^2$ s$^{-1}$) for each tissue type | | | *p*-value[c] | *p*-value[a] | *p*-value[b] |
| --- | --- | --- | --- | --- | --- | --- |
| | Normal[a,b], mean ± SD | Benign[c,a], mean ± SD | Malignant[c,b], mean ± SD | | | |
| 50–1000[d] | 1.87 ± 0.47 | 1.78 ± 0.37 | 1.15 ± 0.47 | <0.001 | 0.01 | <0.001 |
| 50, 200 | 1.86 ± 0.41 | 1.86 ± 0.76 | 1.38 ± 0.61 | <0.001 | 0.92 | <0.001 |
| 50, 400 | 1.83 ± 0.40 | 1.90 ± 0.44 | 1.31 ± 0.54 | <0.001 | 0.17 | <0.001 |
| 50, 600 | 1.80 ± 0.42 | 1.81 ± 0.44 | 1.26 ± 0.49 | <0.001 | 0.37 | <0.001 |
| 50, 800 | 1.76 ± 0.38 | 1.81 ± 0.37 | 1.20 ± 0.48 | <0.001 | 0.05 | <0.001 |
| 50, 1000 | 1.86 ± 0.46 | 1.77 ± 0.37 | 1.15 ± 0.46 | <0.001 | 0.03 | <0.001 |
| 200, 600 | 1.78 ± 0.43 | 1.79 ± 0.48 | 1.22 ± 0.48 | <0.001 | 0.24 | <0.001 |
| 200, 800 | 1.74 ± 0.39 | 1.80 ± 0.39 | 1.16 ± 0.47 | <0.001 | 0.08 | <0.001 |
| 200, 1000 | 1.79 ± 0.47 | 1.76 ± 0.39 | 1.11 ± 0.45 | <0.001 | 0.39 | <0.001 |
| 400, 1000 | 1.71 ± 0.70 | 1.70 ± 0.38 | 1.06 ± 0.45 | <0.001 | 0.74 | <0.001 |

SD, standard deviation.
[a]*p*-value differences in ADC values between normal tissue and solid benign lesions (Mann–Whitney test).
[b]*p*-value differences in ADC values between normal tissue and solid malignant lesions (Mann–Whitney test).
[c]*p*-value differences in ADC values between solid benign and malignant lesions (Mann–Whitney test).
[d]ADC$_{all}$ six *b*-values ranging from 50 to 1000 s mm$^{-2}$.

## Comparison between apparent diffusion coefficient values

Mean ADC values from the *b*-values pairs were compared by lesion histological type (Table 5).

For these combinations of *b*-values, there were no differences between the mean ADC of solid lesions when considering the different histological types.

Figure 3 illustrates a case of a 41-year-old female with a IDC, Grade III and includes sagittal short tau inversion recovery (a), DCE (b), DWI with *b*-value 1000 s mm$^{-2}$ (c) and the ADC map (d).

## DISCUSSION

Reports[15,26] focussing on the best pair of *b*-values to discriminate and characterize breast lesions, particularly when using 3.0 T scanners are scarce. Previous studies[34,35] using few *b*-values (two or three at the most) have reported maximum *b*-values for ADC quantification ranging from 600 to 800 s mm$^{-2}$. Others suggested that more accurate ADC measurements can be achieved by using multiple *b*-values.[8,36] However, in clinical practice, time constraints prevent their use, as acquisition time would otherwise be prolonged. Therefore, it is important to identify a smaller set of *b*-values that enables accurate ADC quantification within a reasonable acquisition time.

Table 3. Relative differences of lesion apparent diffusion coefficient (ADC) values and comparison between ADC values calculated using pairs of *b*-values and ADC$_{all}$

| *b*-values (s mm$^{-2}$) | Mean $\Delta_{rel}$ (%)[a] | Absolute frequency[b] | Relative frequency (%)[c] | *p*-value[d] |
| --- | --- | --- | --- | --- |
| 50, 200 | 27.5 | 4 | 2.6 | <0.001 |
| 50, 400 | 16.8 | 3 | 1.9 | <0.001 |
| 50, 600 | 10.4 | 6 | 3.8 | <0.001 |
| 50, 800 | 5.0 | 23 | 14.7 | <0.001 |
| 50, 1000 | 2.9 | 46 | 29.3 | 0.152[d] |
| 200, 600 | 8.9 | 15 | 9.6 | <0.001 |
| 200, 800 | 5.2 | 27 | 17.2 | 0.866[d] |
| 200, 1000 | 4.6 | 28 | 17.8 | <0.001 |
| 400, 1000 | 9.2 | 5 | 3.2 | <0.001 |

[a]Mean $\Delta_{rel}$: relative difference between ADC and ADC$_{all}$ with respect to ADC$_{all}$, averaged among all lesions.
[b]Absolute frequency: number of lesions for which the ADC value estimated from a particular *b*-value pair is closest to ADC$_{all}$ (smallest $\Delta_{rel}$).
[c]Relative frequency: absolute frequency/total number of lesions.
[d]*p*-value >0.05—no statistical differences between ADC values estimated with the indicated pair and ADC$_{all}$.

Figure 1. Receiver operating characteristic curves when considering *b*-values 50–1000, 50, 1000 and 200, 800 s mm$^{-2}$.
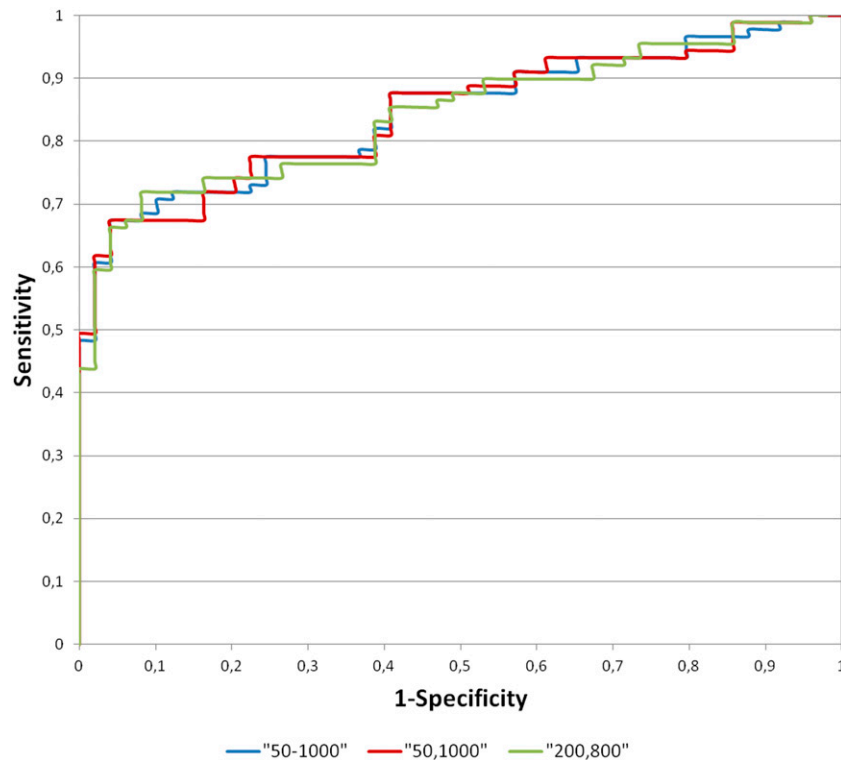


Our results were consistent with previous studies on lesion differentiation.[8,37] The ADC values for malignant lesions were lower than benign ones. The pair 50, 1000 s mm$^{-2}$ provided the ADC estimate closest to ADC$_{all}$. Sensitivity, specificity and accuracy were high (77.5%, 77.6% and 77.5%, respectively), with a probability of a correct diagnosis of 84.4% and the lowest ADC overlap between lesions. The ADC cut-off was $1.46 \times 10^{-3}$ mm$^2$ s$^{-1}$, which is in the range of what was previously reported, although slightly higher when compared with studies using similar pairs of

*b*-values.[25,38] Using the pair 50, 1000 s mm$^{-2}$, mean ADC values were $1.86 \pm 0.46 \times 10^{-3}$ mm$^2$ s$^{-1}$ for normal glandular tissue; $1.77 \pm 0.37 \times 10^{-3}$ mm$^2$ s$^{-1}$ for benign and $1.15 \pm 0.46 \times 10^{-3}$ mm$^2$ s$^{-1}$ for malignant lesions.

Other studies concerning the identification of the best *b*-values for breast lesion discrimination were previously performed at 3.0 T.[15,26] Peters et al[26] used the *b*-values 0, 150, 499, 1500 s mm$^{-2}$ considering five different combinations to measure the diffusion and

Table 4. Diagnostic accuracy when using apparent diffusion coefficient (ADC$_{all}$) or the ADC estimated from the pairs of *b*-values 50, 1000 and 200, 800 s mm$^{-2}$

| Performance metrics | *b*-values pair combinations (s mm$^{-2}$) | | |
|---|---|---|---|
| | 50–1000 | 50, 1000 | 200, 800 |
| ADC cut-off ($\times 10^{-3}$ mm$^2$ s$^{-1}$) | 1.47 | 1.46 | 1.49 |
| Sensitivity (%) | 77.5 | 77.5 | 76.4 |
| Specificity (%) | 75.5 | 77.6 | 73.5 |
| Accuracy (%) | 76.8 | 77.5 | 75.4 |
| AUC (%) | 84.5 | 84.4 | 84.2 |
| AUC (95%) | 77.3–90.0 | 77.3–90.0 | 77.1–89.9 |
| False negative | 20 | 20 | 21 |
| False positive | 10 | 11 | 13 |
| True negative | 58 | 57 | 55 |
| True positive | 69 | 69 | 68 |

AUC, area under the curve.
AUC (95%) indicates the corresponding 95% confidence interval.

Figure 2. Box plots for apparent diffusion coefficient (ADC) values ($\times 10^{-3}$ mm$^2$ s$^{-1}$) for lesion type and normal glandular tissue for ADC$_{all}$ (a), 50, 1000 s mm$^{-2}$ (b) and 200, 800 s mm$^{-2}$ (c). The horizontal lines represent the corresponding ADC cut-off values for differentiating between benign and malignant lesions.
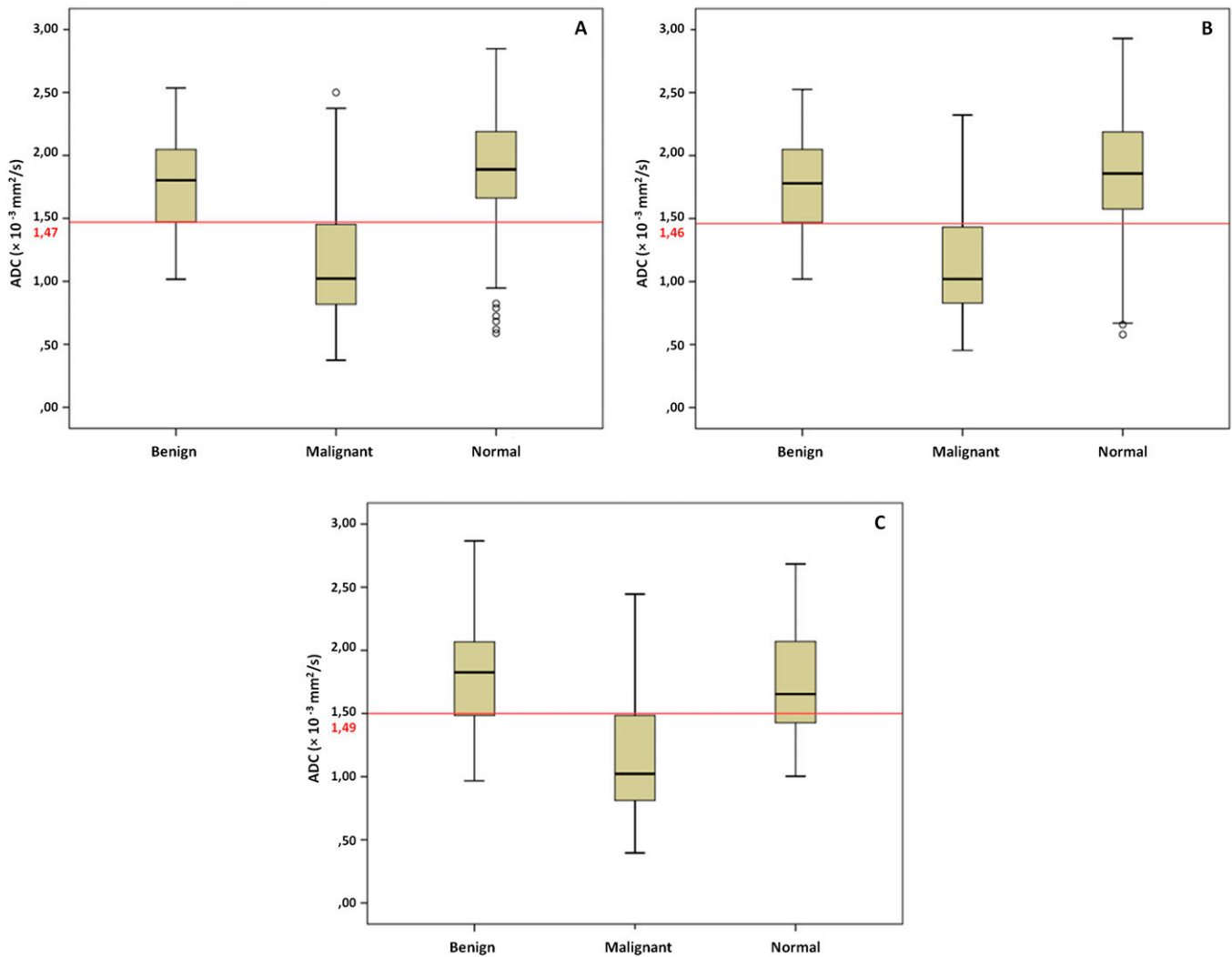


perfusion components. They found that the use of lower or higher *b*-values affects ADC estimates, but not DWI diagnostic performance.

In a similar work, Bogner et al[15] used *b*-values (0, 50, 100, 250, 400, 550, 700, 850, 1000 and 1250 s mm$^{-2}$) and compared sets of pairs. The pair with best accuracy (95%) was 50, 850 s mm$^{-2}$, with similar diagnostic precision to the full *b*-value set. The ADC values we obtained with 50, 1000 s mm$^{-2}$ were similar for normal tissue (Bogner et al:[15] $1.88 \pm 0.24 \times 10^{-3}$ mm$^2$ s$^{-1}$ and the present study: $1.86 \pm 0.46 \times 10^{-3}$ mm$^2$ s$^{-1}$) and malignant lesions (Bogner et al:[15] $1.00 \pm 0.18 \times 10^{-3}$ mm$^2$ s$^{-1}$ and the present study: $1.15 \pm 0.46 \times 10^{-3}$ mm$^2$ s$^{-1}$), with a larger difference seen for benign lesions (Bogner et al:[15] $1.50 \pm 0.27 \times 10^{-3}$ mm$^2$ s$^{-1}$ and the present study: $1.77 \pm 0.37 \times 10^{-3}$ mm$^2$ s$^{-1}$), potentially owing to differences in the specific studied lesions.

In a study developed by Matsuoka et al,[39] malignant lesions in the same patient group were imaged at 3.0 T and 1.5 T; lesions

were classified according to their size as large (>10 mm) or small ($\leq$10 mm). They found that there were no differences in ADC values, which is in agreement with the knowledge that the magnetic field strength has no influence in ADC values. However, visibility in the small lesion group was better at 3.0 T than at 1.5 T, owing to increased SNR and spatial resolution. The mean size of the small lesion group was 6.4 mm (range, 3–10 mm). For this reason, and to ensure appropriate visibility for lesion demarcation and ADC quantification, only lesions with at least 7-mm diameter were included in the present study. Since Peters et al[26] and Matsuoka et al[39] claimed to be able to diagnose tumour lesions with 4 and 3 mm, respectively, using 3.0 T MRI scanners, future studies should test this possibility further and include also smaller lesions in the analysis.

False-positive lesions in this study measured between 8 and 15 mm and comprised 1 PA; 6 FA; 2 CSA; and 2 EPL with fibroblastic/miofibroblastic component. Their small size relative to the voxel dimensions may have impaired their characterization with DWI.

Table 5. Mean apparent diffusion coefficient (ADC) values by histological type for $ADC_{all}$ and the pair combinations of *b*-values 50, 1000 and 200, 800 s mm$^{-2}$

| Histological type | *n* | ADC ($\times 10^3$mm$^2$s$^{-1}$) 50–1000[a,b], mean ± SD | ADC ($\times 10^3$mm$^2$s$^{-1}$) 50, 1000[c,a], mean ± SD | ADC ($\times 10^3$mm$^2$s$^{-1}$) 200, 800[c,b], mean ± SD | *p*-value[c] | *p*-value[a] | *p*-value[b] |
|---|---|---|---|---|---|---|---|
| Ductal Ca *in situ* | 9 | 1.33 ± 0.70 | 1.35 ± 0.69 | 1.30 ± 0.76 | 0.68 | 0.31 | 0.95 |
| Invasive ductal Ca | 47 | 1.05 ± 0.40 | 1.05 ± 0.40 | 1.06 ± 0.40 | 0.75 | 0.51 | 0.55 |
| Lobular Ca *in situ* | 4 | 1.09 ± 0.19 | 1.10 ± 0.20 | 1.05 ± 0.20 | 0.07 | 0.14 | 0.07 |
| Invasive lobular Ca | 20 | 1.30 ± 0.49 | 1.27 ± 0.45 | 1.30 ± 0.43 | 0.12 | 0.06 | 0.44 |
| Mucinous Ca | 1 | 1.47 | 1.38 | 1.39 | – | – | – |
| Other malignant[d] | 8 | 1.21 ± 0.60 | 1.19 ± 0.60 | 1.23 ± 0.61 | 0.58 | 0.21 | 0.89 |
| Fibroadenoma | 24 | 1.80 ± 0.36 | 1.78 ± 0.37 | 1.81 ± 0.38 | 0.46 | 0.32 | 0.77 |
| Epithelial proliferative | 7 | 2.03 ± 0.39 | 2.00 ± 0.36 | 2.05 ± 0.36 | 0.06 | 0.18 | 0.87 |
| Papilloma | 3 | 1.47 ± 0.11 | 1.45 ± 0.08 | 1.47 ± 0.09 | 0.11 | 0.59 | 1.00 |
| Hamartoma | 2 | 1.85 ± 0.48 | 1.82 ± 0.43 | 1.92 ± 0.60 | 0.65 | 0.65 | 0.65 |
| Other benign[e] | 13 | 1.71 ± 0.39 | 1.73 ± 0.39 | 1.70 ± 0.42 | 0.46 | 0.51 | 0.75 |

Ca, carcinoma; *n*, number of lesions; SD, standard deviation.
[a]The *p*-value difference in mean ADC between $ADC_{all}$ and the pair 50, 1000 s mm$^{-2}$ by lesion histological type (Wilcoxon test).
[b]The *p*-value difference in mean ADC between $ADC_{all}$ and the pair 200, 800 s mm$^{-2}$ by lesion histological type (Wilcoxon test).
[c]The *p*-value difference in mean ADC between the pairs 50, 1000 and 200, 800 s mm$^{-2}$ by lesion histological type (Wilcoxon test).
[d]Not otherwise specified.
[e]Fibrocystic changes, complex sclerosing adenosis, complex cystic lesion.

Another possible explanation for the false-positive cases is the presence of fibrotic tissue, proliferation and the degree of cellularity, which restricts water movement and results in lower ADC values. These findings are consistent with other studies.[13,40,41]

False-negative cases were IDC with *in situ* component, highly spread ILC, DCIS and NOS lesions. All these lesions measured between 9 and 29 mm. These results could be related to partial volume effects, specially the ILC owing to the spread of these lesions between tissues, and/or the inadvertent inclusion of areas of necrosis or normal glandular tissue in the ROI, causing elevated ADC estimates. Moreover, the residual presence of blood and/or oedema in the lesions biopsied before MRI could have caused elevated ADC values.

We were able to demonstrate that the choice of *b*-values affects ADC estimates for breast lesions, in agreement with previous studies.[15,25] In this context, it is important to consider the different factors at play when choosing both the minimum and maximum *b*-values, which are now further detailed.

Baron et al[42] showed that the contribution of microperfusion is low in normal breast tissue. However, in malignant processes, angiogenesis is increased to supply tumour growth needs.[43] It is therefore expected that microperfusion effects associated with tumour growth are higher than those observed in normal glandular tissue. Considering that the ADC value is based on the fitting of SI between two or more *b*-values, the attenuation of SI is also dependent on this microperfusion effect. At low *b*-values, microperfusion increases the ADC as observed by Peters et al,[26] and to reduce these effects, the minimum *b*-value in this study was set to 50 s mm$^{-2}$. Although the perfusion contribution was therefore most likely small on our ADC estimates, it is still possible that some contamination effects still remained. To completely remove this effect, some authors suggest the use of minimum *b*-values ranging from 100 to 300 s mm$^{-2}$.[23,44]

Similarly, the choice of maximum *b*-value is also very important. It affects both the accuracy of ADC estimates and lesion conspicuity.[23] Provided a sufficiently high *b*-value is used, signal from normal glandular tissue can be suppressed, with lesions becoming more easily seen. Unfortunately, increasing the maximum *b*-value requires longer TE, resulting in a lower SNR. Since large *b*-values were included in this study (2000 and 3000 s mm$^{-2}$), the number of excitations were increased to compensate for potential SNR losses. Our measured ADC values were similar to those reported in the literature,[29,38] which is consistent with adequate SNR levels. Other factors that may affect the ADC estimates are the mathematical model used, and the type of lesions included in the study.

Our data were acquired and mean SI measured using commercial software provided by the manufacturer. Since there

Figure 3. A 41-year-old female with suspected malignant lesion in the left breast (arrows). Sagittal short tau inversion recovery (a) shows a large lesion, slightly hypointense in comparison with the normal fibroglandular tissue, with intense gadolinium enhancement on the axial dynamic contrast-enhanced acquisition (b). This lesion (c) shows hyperintense signal in the sagittal diffusion-weighted image (*b*-value, 1000 s mm$^{-2}$). The apparent diffusion coefficient (ADC) map (d) shows a hypointense lesion (mean ADC value, $0.664 \times 10^{-3}$ mm$^2$ s$^{-1}$). Histological diagnosis: invasive ductal carcinoma, Grade III.
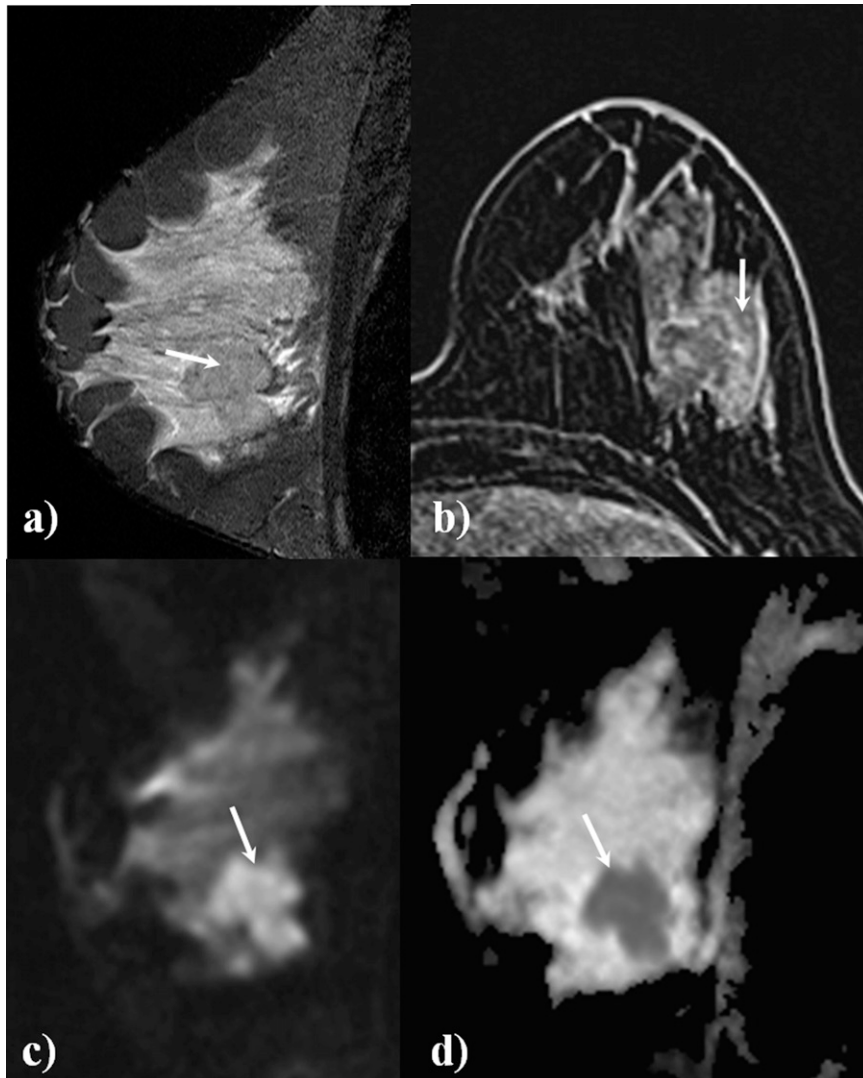


might be differences regarding how image acquisition and re-construction is performed by different manufacturers, care must be taken not to over generalize our results. Further studies should therefore be performed comparing results across manufacturers.

Our study presents some limitations. Firstly, two readers drew the ROIs in consensus, whereas only one reader usually performs it in clinical practice. As mentioned above, the inclusion of high *b*-values in our study prolonged the TE; the consequent decrease in SNR was compensated by increasing the number of repetitions.

Secondly, the ADC of false-negative cases may have been overestimated. A total of 38 lesions were biopsied before MRI. Coincidently, this was true for 16 of the 20 false-negative cases found in this study, namely 7 IDC with *in situ* component, 2 NOS, 6 ILC and 1 DCIS. In these cases, it is possible that the presence of blood and/or oedema could have led to increased ADC values, even if a minimum interval of 10 days was enforced between the biopsy and the subsequent MRI examination. In our breast unit, when lesions present highly suspicious char-acteristics (in mammography and/or echography) the pro-cedure adopted is to perform biopsy before breast MRI. A future study should include a later MRI examination to help determine the minimum period required to avoid such false negatives. Another issue that could explain the observed ADC increase is the partial volume effect that may occur as a result of the slice thickness or the involuntary inclusion of areas of ne-crosis within the ROI.

## CONCLUSION

The *b*-value combinations used influence the estimated ADC values. The best pair of *b*-values, based on ADC quantification, was found to be 50, 1000 s mm$^{-2}$. Sensitivity, specificity and accuracy in lesion discrimination and characterization, considering

an ADC threshold of $1.46 \times 10^{-3}\,\mathrm{mm}^2\,\mathrm{s}^{-1}$, were 77.5%, 77.6% and 77.5%, respectively.

## REFERENCES

1. Sardanelli F, Giuseppetti G, Panizza P, Bazzocchi M, Fausto A, Simonetti G, et al. Sensitivity of MRI versus mammography for detecting foci of multifocal, multicentric breast cancer in fatty and dense breasts using the whole-breast pathologic examination as a gold standard. *AJR Am J Roentgenol* 2004; **183**: 1149–57. doi: 10.2214/ajr.183.4.1831149

2. Kuhl CK, Schrading S, Leutner CC, Morakkabati-Spitz N, Wardelmann E, Fimmers R, et al. Mammography, breast ultrasound, and magnetic resonance imaging for surveillance of women at high familial risk for breast cancer. *J Clin Oncol* 2005; **23**: 8469–76. doi: 10.1200/JCO.2004.00.4960

3. Leach MO, Boggis CR, Dixon AK, Easton DF, Eeles RA, Evans DG, et al. Screening with magnetic resonance imaging and mammography of UK population at high familial risk of breast cancer: a prospective multicentre cohort study (MARIBS). *Lancet* 2005; **365**: 1769–78.

4. Saslow D, Boetes C, Burke W, Harms S, Leach M, Lehman C. American Cancer Society guidelines for breast screening with MRI as an adjunct to mammography. *CA Cancer J Clin* 2007; **57**: 75–89.

5. American College of Radiology.org. *ACR practice guideline for the performance of contrast-enhanced magnetic resonance imaging (MRI) of the breast*. Reston, VA. [Revised 2013, Resolution 12]. Available from: http://www.acr.org/Quality-Safety/Standards-Guidelines

6. Mann R, Kuhl C, Kinkel K, Boetes C. Breast MRI: guidelines from the European Society of Breast Imaging. *Eur Radiol* 2008; **18**: 1307–18. doi: 10.1007/s00330-008-0863-7

7. American College of Radiology (ACR). *Breast imaging reporting and data system atlas (BI-RADS® ) Atlas*. Reston, VA: American College of Radiology; 2003.

8. Guo Y, Cai YQ, Cai ZL, Gao YG, An NY, Ma L, et al. Differentiation of clinically benign and malignant breast lesions using diffusion-weighted imaging. *J Magn Reson Imaging* 2002; **16**: 172–8. doi: 10.1002/jmri.10140

9. Rubesova E, Grell AS, De Maertelaer V, Metens T, Chao SL, Lemort M. Quantitative diffusion imaging in breast cancer: a clinical prospective study. *J Magn Reson Imaging* 2006; **24**: 319–24. doi: 10.1002/jmri.20643

10. Partridge SC, DeMartini WB, Kurland BF, Eby PR, White SW, Lehman CD. Quantitative diffusion-weighted imaging as an adjunct to conventional breast MRI for improved positive predictive value. *AJR Am J Roentgenol* 2009; **193**: 1716–22. doi: 10.2214/AJR.08.2139

11. Partridge SC, Rahbar H, Murthy R, Chai X, Kurland BF, DeMartini WB, et al. Improved diagnosis accuracy of breast MRI through combined apparent diffusion coefficients and dynamic contrast-enhanced kinetics. *Magn Reson Med* 2011; **65**: 1759–67.

12. Roth Y, Ocherashvilli A, Daniels D, Ruiz-Cabello J, Maier SE, Orenstein A, et al. Quantification of water compartmentation in cell suspensions by diffusion-weighted and T2-weighted MRI. *Magn Reson Imaging* 2008; **26**: 88–102.

13. Pereira F, Martins G, Oliveira R. Diffusion magnetic resonance imaging of the breast. *Magn Reson Imaging Clin N Am* 2011; **19**: 95–110. doi: 10.1016/j.mric.2010.09.001

14. Koh DM, Collins DJ. Diffusion-weighted MRI in the body: applications and challenges in oncology. *AJR Am J Roentgenol* 2007; **188**: 1622–35. doi: 10.2214/AJR.06.1403

15. Bogner W, Gruber S, Pinker K, Grabner G, Stadlbauer A, Weber M, et al. Diffusion-weighted MR for differentiation of breast lesions at 3.0T: how does selection of diffusion protocols affect diagnosis? *Radiology* 2009; **253**: 341–51.

16. Sinha S, Sinha U. Recent advances in breast MRI and MRS. *NMR Biomed* 2009; **22**: 3–16. doi: 10.1002/nbm.1270

17. Tsushima Y, Takahashi-Taketomi A, Endo K. Magnetic Resonance (MR) differential diagnosis of breast tumors using apparent diffusion coefficient (ADC) on 1.5-T. *J Magn Reson Imaging* 2009; **30**: 249–55. doi: 10.1002/jmri.21854

18. Partridge SC, DeMartini WB, Kurland BF, Eby PR, White SW, Lehman CD. Differential diagnosis of mammographically and clinically occult breast lesions on diffusion-weighted MRI. *J Magn Reson Imaging* 2010; **31**: 562–70. doi: 10.1002/jmri.22078

19. Koh DM, Takahara T, Imai Y, Collins DJ. Practical aspects of assessing tumors using clinical diffusion-weighted imaging in the body. *Magn Reson Med Sci* 2007; **6**: 211–24.

20. Hiwatashi A, Kinoshita T, Moritani T, Wang HZ, Shrier DA, Numaguchi Y, et al. Hypointensity on diffusion-weighted MRI of the brain related to T2 shortening and susceptibility effects. *AJR Am J Roentgenol* 2003; **181**: 1705–9. doi: 10.2214/ajr.181.6.1811705

21. Woodhams R, Ramadan S, Stanwell P, Sakamoto S, Hata H, Ozaki M, et al. Diffusion-weighted imaging of the breast: principles and clinical applications. *Radiographics* 2011; **31**: 1059–84. doi: 10.1148/rg.314105160

22. Le Bihan D, Breton E, Lallemand D, Aubin ML, Vignaud J, Laval-Jeantet M. Separation of diffusion and perfusion in intravoxel incoherent motion MR imaging. *Radiology* 1988; **168**: 497–505.

23. Koh DM, Collins DJ, Orton MR. Intravoxel incoherent motion in body diffusion-weighted MRI: reality and challenges. *AJR Am J Roentgenol* 2011; **196**: 1351–61. doi: 10.2214/AJR.10.5515

24. Tamura T, Usui S, Murakami S, Arihiro K, Akiyama Y, Naito K, et al. Biexponential signal attenuation analysis of diffusion-weighted imaging of breast. *Magn Reson Med Sci* 2010; **9**: 195–207.

25. Vermoolen M, Nievelstein K. Apparent diffusion coefficient measurements in the differentiation between benign and malignant lesions: a systematic review. *Insights Imaging* 2012; **3**: 395–409. doi: 10.1007/s13244-012-0175-y

26. Peters NH, Vincken KL, Van den Bosch MA, Luijten PR, Mali WP, Bartels LW. Quantitative diffusion weighted imaging for differentiation of benign and malignant breast lesions: the influence of the choice of b-values. *J Magn Reson Imaging* 2010; **31**: 1100–5. doi: 10.1002/jmri.22152

27. Tozaki M, Fukuma E. 1H MR spectroscopy and diffusion-weighted imaging of the breast: are they useful tools for

characterizing breast lesions before biopsy? *AJR Am J Roentgenol* 2009; **193**: 840–9. doi: 10.2214/AJR.08.2128

28. Ochi M, Kuroiwa T, Sunami S, Murakami J, Miyahara S, Nagaie T, et al. Diffusion-weighted imaging (b value=1500 s/mm$^2$) is useful to decrease false-positive breast cancer cases due to fibrocystic changes. *Breast Cancer* 2013; **20**: 137–44.

29. Orguc S, Basara I, Coskun T. Diffusion-weighted MR imaging of the breast: comparison of apparent diffusion coefficient values of normal breast tissue with benign and malignant breast lesions. *Singapore Med J* 2012; **53**: 737–43.

30. Partridge SC, McKinnon GC, Henry RG, Hylton NM. Menstrual cycle variation of apparent diffusion coefficients measured in the normal breast using MRI. *J Magn Reson Imaging* 2001; **14**: 433–8.

31. Tamura T, Usui S, Murakami S, Arihiro K, Fujimoto T, Yamada T, et al. Comparisons of multi b-value DWI signal analysis with pathological specimen of breast cancer. *Magn Reson Med* 2012; **68**: 890–7. doi: 10.1002/mrm.23277

32. Jensen JH, Helpern JA, Ramani A, Lu H, Kaczynski K. Diffusion Kurtosis imaging: the quantification of non-gaussian water diffusion by means of magnetic resonance imaging. *Magn Reson Med* 2005; **53**: 1432–40.

33. Chatterjee S, Hadi AS. Simple linear regression. In: Chatterjee S, Hadi AS, ed. *Regression analysis by example*. 4th edn. NJ, Hoboken: John Wiley & Sons, Inc; 2006. pp. 28–32.

34. Rahbar H, Partridge SC, Eby PR, DeMartini WB, Gutierrez RL, Peacock S, et al. Characterization of ductal carcinoma in situ on diffusion weighted breast MRI. *Eur Radiol* 2011; **21**: 2011–19. doi: 10.1007/s00330-011-2140-4

35. Koh DM, Blackledge M, Burns S, Hughes J, Stemmer A, Kiefer B, et al. Combination of chemical suppression techniques for dual suppression of fat and silicone at diffusion-weighted MR imaging in women with breast implants. *Eur Radiol* 2012; **22**: 2648–53. doi: 10.1007/s00330-012-2531-1

36. Bonekamp S, Corona-Villalobos C, Kamel I. Oncologic applications of diffusion-weighted MRI in the body. *J Magn Reson Imaging* 2012; **35**: 257–79. doi: 10.1002/jmri.22786

37. Kul S, Cansu A, Alhan E, Dinc H, Gunes G, Reis A. Contribution of diffusion-weighted imaging to dynamic contrast-enhanced MRI in the characterization of breast tumors. *AJR Am J Roentgenol* 2011; **196**: 210–17. doi: 10.2214/AJR.10.4258

38. Hatakenaka M, Soeda H, Yabuuchi H, Matsuo Y, Kamitani T, Oda Y, et al. Apparent diffusion coefficients of breast tumors:

clinical application. *Magn Reson Med Sci* 2008; **7**: 23–9.

39. Matsuoka A, Minato M, Harada M, Kubo H, Bandou Y, Tangoku A, et al. Comparison of 3.0- and 1.5-tesla diffusion-weighted imaging in the visibility of breast cancer. *Radiat Med* 2008; **26**: 15–20.

40. Kinoshita T, Yashiro N, Ihara N, Funatu H, Fukuma E, Narita M. Diffusion-weighted half-Fourier single-shot turbo echo imaging in breast tumors: differentiation of invasive ductal carcinoma from fibroadenoma. *J Comput Assist Tomogr* 2002; **26**: 1042–6.

41. Brandão AC, Lehman CD, Partridge SC. Breast magnetic resonance imaging: diffusion-weighted imaging. *Magn Reson Imaging Clin N Am* 2013; **21**: 321–36.

42. Baron P, Dorrius MD, Kappert P, Oudkerk M, Sijens PE. Diffusion-weighted imaging of normal fibroglandular breast tissue: influence of microperfusion and fat suppression technique on the apparent diffusion coefficient. *NMR Biomed* 2010; **23**: 399–405. doi: 10.1002/nbm.1475

43. Bowden D, Barret T. Angiogenesis imaging in neoplasia. *J Clin Imaging Sci* 2011; **1**: 1–7.

44. Thoeny HC, De Keyzer F. Extracranial applications of diffusion-weighted magnetic resonance imaging. *Eur Radiol* 2007; **17**: 1385–93. doi: 10.1007/s00330-006-0547-0